Noname manuscript No.
(will be inserted by the editor)

Automatic evaluation of vessel diameter variation from 2D X-ray angiography

Faten M'hiri · Luc Duong · Christian Desrosiers · Nagib Dahdah · Joaquim Miró · Mohamed Cheriet ·

Received: date / Accepted: date

Abstract Purpose: Early detection of blood vessel pathologies can be made through the evaluation of functional and structural abnormalities in the arteries, including the arterial distensibility measure. We propose a feasibility study on computing arterial distensibility automatically from monoplane 2D X-ray sequences.
Methods: To compute the distensibility measure, three steps were developed: First, the segment of an artery is extracted using our graph-based segmentation method. Then, the same segment is tracked in the moving sequence using our spatio-temporal segmentation method: the Temporal Vessel Walker. Finally, the diameter of the artery is measured automatically at each frame of the sequence based on the segmentation results.
Results: The method was evaluated using one simulated sequence and 4 patients' angiograms depicting the coronary arteries and three depicting the ascending aorta. Results of the simulated sequence achieved a Dice index of 98%, with a mean squared error in diameter measurement of 0.18 ± 0.31mm. Results obtained from patients' X-ray sequences are consistent with manual assessment of the diameter by experts.
Conclusions: The proposed method measures changes in diameter of a specific segment of a blood vessel during the cardiac sequence, automatically based on monoplane 2D X-ray sequence. Such information might become a key to help

This research was funded by the Fonds de recherche du Quebec Nature et technologies FQRNT (www.fqrnt.gouv.qc.ca) and the Natural Sciences and Engineering Research Council of Canada NSERC (www.nserc-crsng.gc.ca).

F. M'hiri (✉) · L. Duong · C. Desrosiers
Departement of Software and IT Engineering, École de technologie supérieure, Montreal, Canada
E-mail: faten.mhiri.1@ens.etsmtl.ca

N. Dahdah · J. Miró
Department of Cardiology, Sainte-Justine Hospital, Montreal, Canada

M. Cheriet
Automated Production Engineering, École de technologie supérieure, Montreal, Canada

Article published in the *International Journal of Computer Assisted Radiology and Surgery* (JCARS), vol. 12, Iss. 11, p. 1867–1876
https://doi.org/10.1007/s11548-017-1639-9

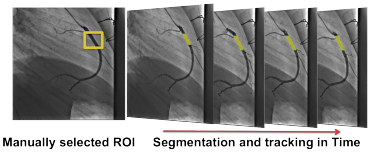

Fig. 1 Segmentation and tracking of a section of a coronary artery as defined by a manually selected region of interest.

physicians in the detection of variations of arterial stiffness associated with early stages of various vasculopathies.

Keywords Segmentation · Tracking · Coronary arteries · Artery elasticity · X-ray angiography · Vessel width

1 Introduction

Early detection of blood vessel anomalies can improve treatment for cardiovascular pathologies such as Kawasaki disease, heart transplant rejection or arteriosclerotic vascular disease. Such pathologies affect the elasticity of coronary arteries (CAs) [26]. The elasticity of CAs during the cardiac cycle is used to assess vascular function and to help with diagnosis and treatment. The distensibility measure is one of the most accurate indicators of elasticity and of any potential cardiovascular disease at an early stage [6]. This measure computes the correlation between a vessel's change in diameter during systole and diastole with variations in blood pressure. The accurate measurement of a blood vessel's diameter from 2D X-ray angiograms is critical to compute distensibility. An optimal procedure to assist cardiologists is to: 1) segment the section of the vessel of interest; 2) track the same section of the vessel in the moving sequence; and 3) compute its diameter in each frame. All these steps should occur automatically, as illustrated in Fig.1.

Extracting, tracking, and measuring the diameter of arteries from moving sequences is a challenging task. First, segmenting arteries can depend on the nature of the artery and the imaging modality. An exhaustive literature review on the subject has been conducted previously [14]. Different approaches have been proposed to address the challenges of segmenting blood vessels. They are either based on variational approaches such as level sets [28], or on graph-based methods such as graph cuts [23], or random walks [29]. In the current study, we used a method we developed called Vessel Walker [17] that extends the random walks method [10] to segment blood vessels. Second, vessels like coronary arteries are subject to a combination of cardiac and respiratory motions, which are challenging to model, as observed by Shechter *et al.* [24]. Also, clinicians need to be able to evaluate a specific part of an artery. Existing solutions track all the vessels in the sequence, such as the entire coronary tree. This can be useful to detect the presence of stenosis [7] but not to evaluate the elasticity of a specific segment of an artery. In this study we focused on tracking and evaluating a segment of the artery within a specific region of interest (ROI) as determined by a cardiologist. This can be challenging, since the segment is a dark tubular structure similar to all the arteries displayed in the sequence. In this paper, we present our Temporal Vessel Walker method (TVW), previously described in [18], to track a specific part of an artery

using temporal priors. Third, diameter changes in the cardiac cycle can be very small (less than 1mm for coronary arteries). Therefore, a precise measurement tool that can capture very small changes in diameter is needed. Finally, an automatic method needs to be able to return robust results when dealing with both small arteries (such as coronary arteries) and larger arteries (such as the aorta).

Computing distensibility usually involves manual diameter measurements at specific locations in one or two frames in the angiographic sequence. However, such a procedure can be time consuming and can lead to important inter-observer and intra-observer variability [25]. Other measurement techniques are proposed in the literature or with existing software [11,21,16] to semi-automatically segment part of a vessel from a single frame. To the best of our knowledge, these methods do not include a temporal analysis of diameter variation; neither do they track the vessel in the moving sequence. In addition, existing works that evaluate distensibility are applied to other imaging modalities, such as ultrasound images [15], CT images [2], or MRI [12]. Studies on quantifying arterial structures based on 2D X-ray angiograms do not present fully automatic tracking of the diameter of a specific part of an artery in the cardiac sequence. Some of these methods usually use a 3D reconstructed model from biplane views to evaluate the vessel's width [9].

Few groups have studied the correlation between the assessment of coronary artery distensibility from 2D angiography sequences and the detection of pathologies using automatic centerline extraction and diameter estimation [4,3]. The current research explores automatic computation of diameter variations of large and small blood vessels from monoplane 2D X-ray sequences. We introduce a new method to measure changes in diameter of a specific segment of a blood vessel during the cardiac sequence, *automatically* based on *monoplane 2D X-ray sequence*. The method was validated using simulated sequences and data from patients displaying coronary arteries and the ascending aorta.

2 Materials and methods

Fig. 1 describes the steps of the proposed method. First, a ROI surrounding a section of an artery is selected (left image in Fig.1). Then, the artery within the ROI is segmented and tracked using our proposed method, described in the following section. Finally, the mean diameter of the extracted artery is computed at each frame, and is described in section 2.2. Our final results are compared with manual measurements and with the Mirzaalian's method [19]. The latter method uses a graph-based method and a Markov random field to assess blood vessel scale.

2.1 Segmentation and tracking of a section of artery

In the first frame of the 2D X-ray sequence, the section of the vessel is segmented using our Vessel Walker (VW) segmentation method [17]. This method extracts vessels in X-ray images by combining a graph-based representation and vesselness features. These features are computed using a hessian-based filter [8], which assigns to each pixel a probability-like value that it belongs to a tubular structure. Using the Vessel Walker result, the vessel within the selected ROI is extracted. The same extracted section of a vessel has to be tracked in the rest of the frames. Our idea

is to use the segmentation result in one frame to segment the following frame. To do so, we extend our previous Vessel Walker method to guide the segmentation of the same structure in the sequence using previous segmentation results. This lead to the Temporal Vessel Walker method, described previously in [18].

Having the segmentation result $\boldsymbol{f}^{t-1}$ from the previous frame $\mathcal{I}^{t-1}$ at time $(t-1)$, the TVW method computes the segmentation result $\boldsymbol{f}$ at the current frame $\mathcal{I}^t$ at time t. The optimal solution $\boldsymbol{f}$ is a mapping $\boldsymbol{f} : \mathcal{I}^t \rightarrow \{0, 1\}$, where $f_i = 1$, if the pixel i belongs to the vessel, and $f_i = 0$, if i belongs to the background. The method is defined as the minimization of the following energy equation:

$$\begin{aligned} E(\boldsymbol{f}) \; = \frac{1}{2}\sum_{i=1}^{|\mathcal{I}|}\sum_{j=1}^{|\mathcal{I}|} w_{ij}(f_i - f_j)^2 \; + \; \alpha\sum_{i=1}^{|\mathcal{I}|}(1-b_i)f_i^2 \; + \; \beta\sum_{i=1}^{|\mathcal{I}|} b_i(f_i-1)^2 \\ + \mu\sum_{i=1}^{N}\sum_{j=1}^{N} w_{\tau ij}(\boldsymbol{f}_j - \boldsymbol{f}_i^{t-1})^2 \end{aligned} \tag{1}$$

In this equation, frame $\mathcal{I}^t$ is represented by graph $G = \{N, E\}$, with node set N representing all pixels in the image. Each pair of neighboring nodes is connected by an edge with a weight w_{ij} expressing the intensity similarity between the nodes. The value of $b_i \in [0, 1]$ expresses the vesselness feature of a pixel i computed using Frangi's filter [8], which assigns a probability-like value that a pixel belongs to a vessel. Parameters $\alpha, \beta \geq 0$ are used to control the trade-off between minimizing the vesselness of background pixels and maximizing the vesselness of foreground pixels. Parameter μ controls the weight of temporal prior information in the final segmentation result. The obtained result $\boldsymbol{f}$ assigns to each pixel a probability that it belongs to the foreground. To get a binary segmentation, Ostu's [20] thresholding method is applied on vector $\boldsymbol{f}$.

In the context of this study, as we aimed to track a specific part of the artery, a length constraint needs to be considered. Because the TVW formulation does not control for such a constraint, we added an intensity-based rigid registration step: After computing the TVW result, the segmentation mask from the previous frame f^{t-1} is aligned on the TVW result f. The sections from f that do not overlap with f^{t-1} are deleted. Finally, for each segmented frame and to limit background noise, a post-processing step is applied to get only the biggest connected component as the final segmentation result.

2.2 Measuring a vessel's diameter

The proposed approach is a modified version of an existing one [7] to compute a vessel's diameter. After extracting the part of the vessel in the moving sequence, the mean diameter at each frame is measured. The method starts by extracting the centerline of the vessel using the Hamilton-Jacobi skeleton [5], as shown in the left image in Fig. 2. The Hamilton-Jacobi method is well known for its accuracy in extracting centerlines homotopic to the original objects. It has been proved to be computationally efficient and robust to boundary noise. The vesselness filter is used again at this step to locate the vessel's direction at each point on the image. To measure the vessel's width, the vesselness vector for each centerline point is computed using the Frangi method [8]. This vector indicates, at each point of

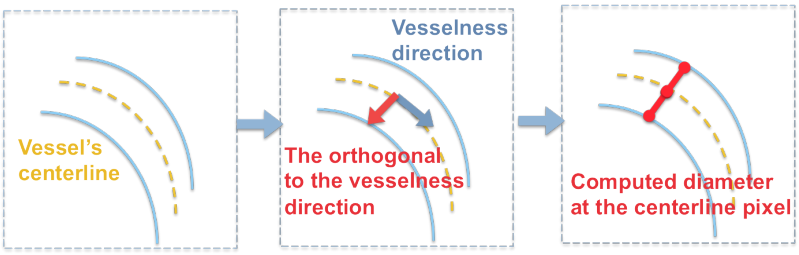

Fig. 2 The different steps to compute a vessel's diameter

the centerline, the direction of the vessel. Following the direction normal to the vesselness vector at one point, the method looks for the boundary pixels on either side of the centerline, as illustrated in the middle image in Fig. 2. The diameter of the vessel is computed as the sum of the distances between each centerline point and its corresponding boundary pixel from two sides of the centerline, as in the right image in Fig. 2.

The method computes the diameter for every centerline point. Such information can be valuable for identifying local deformation within the vessel, such as stenosis. In the context of this study, the mean diameter of the selected segment is considered.

2.3 Imaging data

To evaluate the proposed method, three datasets were selected:

1. **Simulated data:** One simulated X-ray sequence displaying the coronary artery tree. The sequence was acquired with the XCAT phantom, developed by Carl E. Ravin Advanced Imaging Laboratories [22]. The XCAT provides a realistic view of coronary arteries in 2D X-ray angiography. The sequence displays in 69 frames, right and left coronary arteries moving under respiratory and cardiac motions. Ground truth segmentation masks of the artery are provided using the XCAT system, this is used to evaluate the segmentation accuracy of the proposed TVW method.
2. **Patient data:** Seven 2D X-ray sequences of young patients were acquired from Sainte-Justine Hospital (Montreal, Canada). The data were acquired using a C-arm Infinix-CFI BP by Toshiba. They were anonymized into the DICOM format, and were recorded after approval by the Sainte-Justine Institutional Ethics Review Board. These angiograms display coronary arteries and the ascending aorta:
   (a) Four 2D X-ray sequences of young patients displaying coronary arteries. Ground truth segmentation masks are not provided. However, two X-ray sequences have corresponding manual diameters measured by one clinical expert at one frame.
   (b) Three X-ray sequences displaying the ascending aorta of three young patients. To evaluate diameter computations of the proposed method, the width of the ascending aorta was manually measured by an experienced user at each frame. Knowing that the aorta can be much larger than a

coronary artery, the degree of manual measurement error can be smaller. Therefore, these manual measurements are used to validate diameter computations.

The following experiments evaluated segmentation, tracking, and width measurements of coronary arteries and the aorta on simulated and patient X-ray sequences.

3 Results

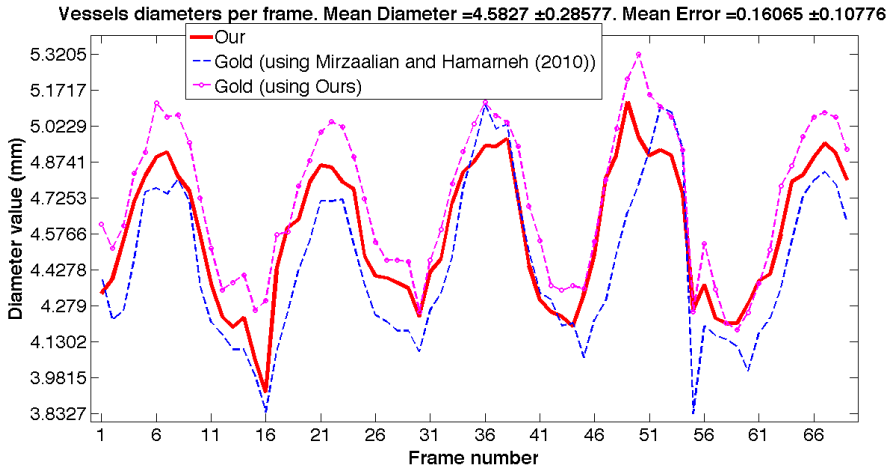

Fig. 3 Diameter measurements of the targeted section of the vessel at each of the 69 frames of the simulated sequence. Red curve: Temporal Vessel Walker segmentation results with our proposed diameter measurements. Pink curve: Diameter measured using our diameter computation method on ground truth segmentation masks provided by the XCAT system. Blue curve: Diameter measured using the Mirzaalian method [19] on ground truth segmentation masks.

3.1 Results using the simulated coronary arteries sequence

The proposed method was evaluated using the simulated X-ray sequence. The objective was to evaluate the accuracy of the method in segmenting, tracking, and measuring a section of a right coronary artery. We used the Dice index to assess the overlap of our results with the ground truth mask provided using the XCAT system. Mean performance of the method had a high Dice value of 0.98 with a precision result of 1 and recall of 0.96. Such results confirm the accuracy and robustness of the proposed method in segmenting and tracking the section of the artery in all 69 frames of the sequence. Because ground truth results in terms of vessel diameter in the sequence were not available, the vessel's width from ground truth masks were computed using our diameter approach and using the method proposed by Mirzaalian and Hamarneh [19]. We compared these measurements to

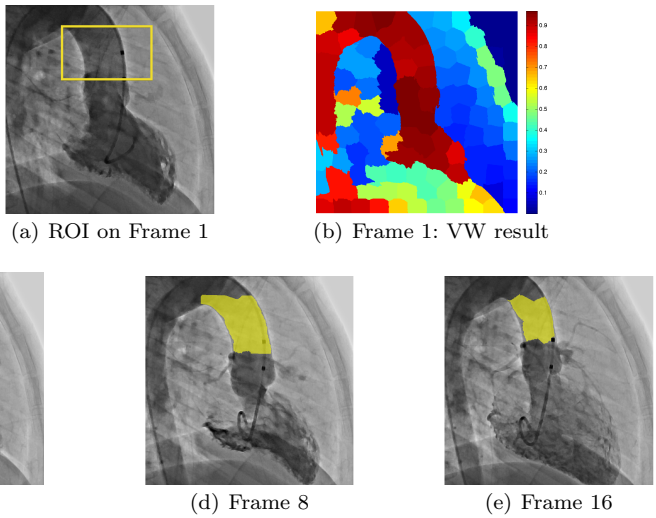

(a) ROI on Frame 1 (b) Frame 1: VW result

(c) Frame 1 (d) Frame 8 (e) Frame 16

Fig. 4 Results from the second sequence of our dataset displaying the ascending aorta. (**a**) The defined region of interest (ROI) in the first frame of the sequence. (**b**) Results of the Vessel Walker method in the first frame. The method assigns a probability value to each pixel that it belongs to the foreground. (**c**) Binary segmentation result of the Vessel Walker method within the ROI. (**d**) and (**e**) Segmentation results of the TVW method in frame 8 and 16 of the sequence.

our TVW method. Fig. 3 shows the different diameter measurements of the section of right coronary artery in the simulated sequence. The three curves have a similar pattern, with diameter values close to each other. Our computed mean diameter (over the temporal sequence of 69 frames) was 4.58 ± 0.29mm. Comparing our results (red curve) with ground truth measurements using the Mirzaalian's method (blue dashed curve) gives a mean squared error of 0.16 ± 0.11mm. Comparing our results with the ground truth measurements using our measurement approach (pink dotted curve) gives a mean squared error of 0.18 ± 0.31mm. Both errors are relatively low, and our method succeed in measuring the diameter while capturing small diameter changes.

Despite differences in diameter measurements among the three curves, they all show the same pattern repeated five times. This pattern corresponds to five cardiac cycles simulated by the sequence. The three curves capture the same diameter changes in systole and diastole, which confirms the hypothesis that it is possible to capture small changes in an artery's diameter from 2D X-ray sequences. More tests are required to assess the precision of our diameter measurements. The following section evaluates this precision.

3.2 Results using patients sequences

3.2.1 Results using an aorta dataset

The proposed method was tested on three sequences displaying the aorta. The aorta is a large blood vessel with big diameter variations during the cardiac cy-

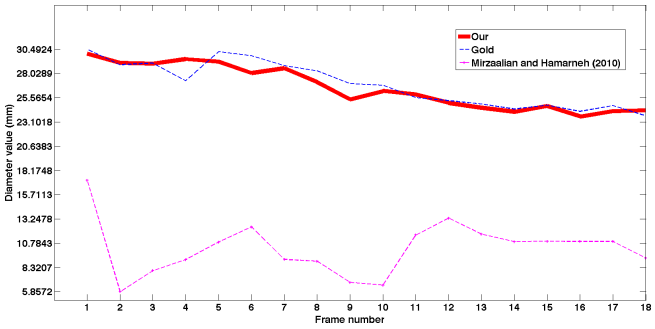

Fig. 5 Diameter values of the second sequence displaying the ascending aorta using the proposed method and the Mirzaalian method, compared with ground truth values.

cle. Sequences showing the ascending aorta were selected and their corresponding diameters were manually computed. Due to a much larger diameter compared to coronary arteries, the degree of manual measurement error is expected to be lower.

Sequences displaying the aorta have low contrast compared with coronary artery sequences. Therefore, the intensity level is inhomogeneous in the aorta and the contrast with the image's background is low. To enhance the contrast level in the frame, an anisotropic filter [27, 13] is applied to enhance intensity homogeneity within the aorta, while limiting noise level. Additionally, superpixel computation [1] was added as a pre-processing step to simplify the segmentation and tracking steps. The superpixel method defines small groups of similar pixels. It is an over-segmentation method that ensures that similar pixels stay connected, while respecting the object's boundaries. Because the contrast in these images can be limited and the intensity level inside the aorta can be inhomogeneous, the superpixel method helps create large groups of similarly connected pixels, making segmentation and tracking more accurate. Moreover, using the superpixel method simplifies the design of graph G used in equation (1) by considering each superpixel as one node of the graph (instead of considering each pixel as a node in graph G). Furthermore, the registration step is skipped because the motion of the aorta is not as large as the motion of coronary arteries.

Fig. 4(a) displays the selected ROI in the second sequence of our dataset. Fig. 4(b) shows the probabilities assigned by the Vessel Walker method to each pixel in the frame. The method accurately highlights the aorta (red colored regions showing high probabilities that they belong to the aorta) from the background (blue colored regions showing low probabilities). Using this result, the segmentation mask is computed within the specified ROI. The result in the first frame is displayed in yellow in Fig. 4(c). The segmentation and tracking results in the other frames (Fig. 4(d) and 4(e)) using TVW and superpixels show that the method succeeds in extracting and tracking the specified part of the ascending aorta.

Figure 5 shows mean diameter of the ascending aorta computed at each frame of the sequence. It displays the diameter variation curve using our approach (red curve) compared with ground truth manual measurements (blue dashed curve) and the diameter computed using the Mirzaalian method [19] (pink dotted curve). Our measurements are close to the ground truth measurements with the mean

Table 1 Mean diameter measurement (in mm) using the proposed method and the Mirzaalian method, with the corresponding mean squared error computed in each sequence of the aorta dataset.

Seq.	**Diameter (TVW)**	**Diameter using [19]**	**MSE (TVW)**	**MSE [19]**
1	41.6± 2.6	12.3 ±2.7	2.1± 2.2	27.4± 1.6
2	26.6± 2.2	10.3 ±2.7	0.7 ± 0.6	16.7 ± 3.5
3	26.5± 2.0	14.7 ±2.6	1.7± 1.8	10.1± 2.9
Mean	31.6	12.4	1.5	18.1

squared error was 0.7 ± 0.6 mm. The proposed diameter measurement method performs better than the Mirzaalian method.

Table 1 shows mean diameter results over each sequence of the aorta dataset. The first and second columns of the table show the diameter computed using our method and the Mirzaalian method. The third and fourth columns show the corresponding mean squared error (MSE) between our measurements and manual ground truth measurements and between Mirzaalian measurements and ground truth. The results indicate that the proposed method returns a better performance (mean MSE= 1.5mm) compared with the Mirzaalian method (mean MSE= 18.1mm). This is explained by the Mirzaalian method working accurately on thin vessels but not adapting to compute the scale of large vessels like the aorta. Our method, however, can compute accurately the scales of both thin and large vessels.

3.2.2 Results using a coronary artery dataset

The proposed approach was tested on four angiographic sequences displaying coronary arteries. For the first sequence, the diameter was manually measured. While these manual measurements may be not as precise as those taken for the aorta, they can be used as a general indicator of the performance of the proposed method.

Fig. 6 shows the computed diameter values per each frame for the first sequence. The curves from manual measurements (blue dashed curve) and the proposed method (red curve) are similar to each other and have measurements in common (for example, at frames 9 and 26). This is further shown by a mean squared error of 0.52 ± 0.35mm. The proposed measurement method performs better than the Mirzaalian method [19], where its curve is far below the manual result, with a mean squared error of $= 1.19 \pm 0.67$mm.

Manual measurements by a clinician were provided in one frame from the second and fourth sequence. Fig. 7(a) shows manual measurements of the artery made by a clinician on the fourth sequence of the dataset. The rest of the images in Fig. 7 show the manually specified ROI in the first frame of the fourth sequence of our dataset with the computed segmentation results overlaid in yellow on four frames of the sequence. The segmentation results are encouraging because they track accurately the specified section of the vessel despite the presence of cardiac and respiratory motions. The computed mean diameter using our method was 3.08 ± 0.2mm, which is close to the diameter measured around region B in image

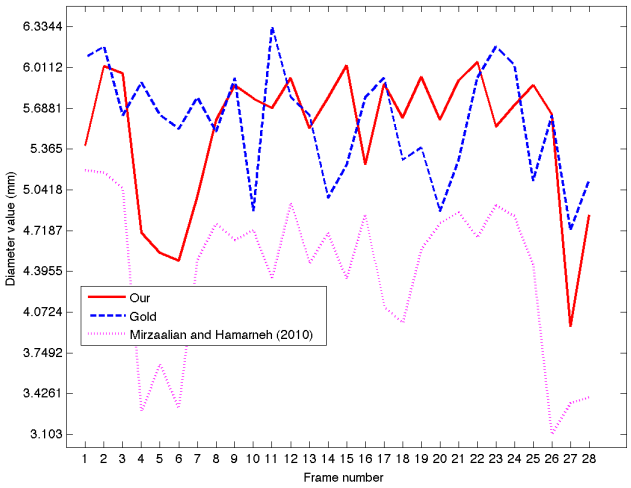

Fig. 6 Diameter values per frame using the proposed approach and the Mirzaalian method compared with manual measurements in the first sequence displaying a coronary artery.

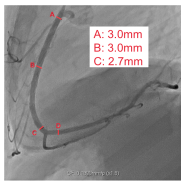

(a) Manual measurements of the RCA

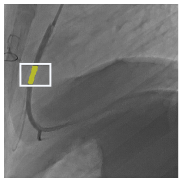

(b) Frame 1 showing the ROI (white box)

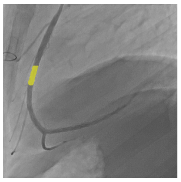

(c) Frame 5

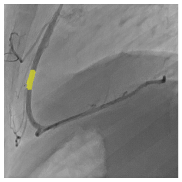

(d) Frame 15

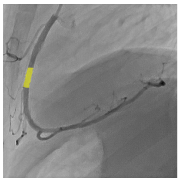

(e) Frame 25

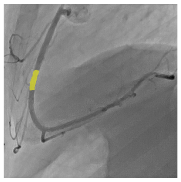

(f) Frame 50

Fig. 7 Segmentation results of the region of interest (ROI) in the right coronary artery (RCA) at four frames in the fourth sequence.

7(a), with a measurement of 3mm, indicating again the accuracy of the proposed method.

Fig. 8 shows the computed diameter in each frame of the second sequence of the dataset with its corresponding electrocardiography (ECG) signal at the bottom (left). The diameter values decrease and then increase depending on changes in the ECG signal. The diameter curve starts with a maximum value at the first three frames of the sequence and decreases after frame 4. The decrease in diameter happens at the first spike in the ECG signal (near the QRS complex), which corresponds to the systole phase of the cardiac cycle. At that time, the myocardium is contracting and blood flow is limited in the coronary arteries. After the first

peak, the diameter starts to increase again around frame 10 of the sequence. This corresponds with the ECG signal for diastole, when the myocardium relaxes and coronary artery flow increases. The diameter curve reaches a maximum before the second spike in the ECG signal. This shows that the proposed automatic method can capture the diameter variation corresponding to the cardiac cycle. The image on the right in Fig. 8 shows that the diameter manually measured around segments A and B is 1.9mm, which is close to our computed mean diameter value of 1.555 ± 0.13mm.

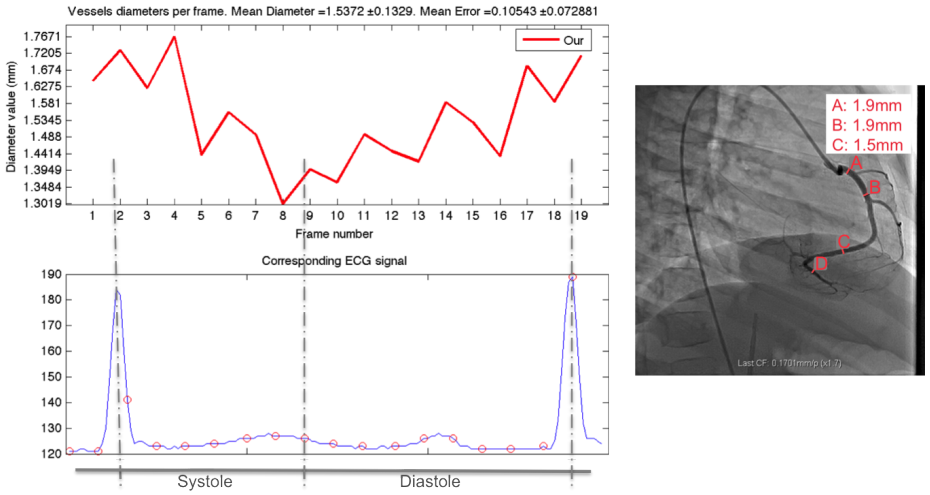

Fig. 8 Left: Diameter values per frame using the proposed approach in the second sequence of the coronary artery dataset with the corresponding electrocardiography signal (blue curve with the red circles; circles correspond to frame acquisition times). Right: Manually computed diameter by a medical expert from Sainte-Justine Hospital.

4 Discussion and conclusion

Computing the properties of blood vessels is of crucial importance in order to detect pathologies. Our method focuses on computing diameter changes that occur in a specific segment of a blood vessel, such as the coronary arteries or the aorta, automatically from 2D X-ray sequences.

Tracking a section of a vessel in X-ray sequences can be error-prone. This is because a segment of vessel is a dark tubular structure similar to all blood vessels displayed in the sequence. Using our proposed TVW method, we were able to overcome the problems associated with tracking a section of vessel. Fig. 4 and 7 show how, starting from a specified ROI, the method extracts and tracks accurately the section of the vessel. Methods like that proposed by Compas *et al.* [7] track and compute diameter changes in a coronary artery tree to detect stenosis in the vessels but do not show diameter variations at a specific location of the tree.

With regard to the estimation of a vessel's width, the Mirzaalian method [19] has shown successful results on a retinal vessel dataset. That method optimizes the

assignment of scale labels to each part of the vessel. It enhances the scale values computed using the Frangi vesselness filter [8]. However, as shown in Table 1, the method seems to perform better on thin vessels rather than larger ones such as the aorta. In contrast, our proposed method is more accurate at computing the diameter of both large and thin vessels.

The accuracy of our TVW method was tested on simulated data. Results indicated the precision of the method in segmenting and tracking the correct segment of interest, despite respiratory and cardiac motions. The simulated data were of five different cardiac cycles. Fig. 3 shows that our proposed method was able to capture diameter changes accurately through the the cardiac cycle. The computed diameter variability was also in agreement with the ground truth result. Tests on patients' coronary angiographies (Fig. 8) showed that the diameter changes evolved with the corresponding ECG signal. An increase in diameter coincided with the heart relaxation phase, when the flow in the coronary arteries is maximal, and the same artery showed a decrease with heart contraction. These results are encouraging and indicate that distensibility can be measured directly from monoplane 2D X-ray sequences. Other studies [4, 3] have reported on the correlation between diameter measurements from 2D angiograms with pathology scoring. It is suggested that our proposed method could be used for the detection of variation of arterial stiffness, which could represent early stages of arterial disease in conditions such as atherosclerosis of large and small vessels, Kawasaki disease or vascular rejection following solid organ transplantation (heart, kidney, liver, etc). Further clinical studies are required to validate this suggestion.

Future work will focus on enhancing the robustness of the TVW method to the motion of the coronary arteries in the moving sequence. A length term and a curvature term should be added to the model to ensure that the method is tracking the segment of the same length in the sequence. Finally, other diameter measurement approaches should be considered to enhance the precision of the computations.

In conclusion, the TVW method was evaluated for its ability to segment and track a specific part of a blood vessel in 2D X-ray sequences. The results show the method was able to capture diameter changes in the artery according to heart contraction and relaxation. The performance of the proposed method showed accuracy in segmenting, tracking, and measuring diameter variation in coronary arteries and the ascending aorta. Experimental tests were applied using simulated and real sequences of coronary arteries and on sequences displaying the ascending aorta. Results were encouraging for this method's ability to track the right section of the artery and for measuring diameter variations accurately. The method was able to capture diameter changes in both large and thin vessels, which aligned with systole and diastole.

This proposed automatic method appears effective and efficient at segmenting, tracking, and measuring a blood vessel's diameter from monoplane 2D X-ray sequences. Such information might become a key to help physicians in the detection of variations of arterial stiffness associated with early stages of various vasculopathies.

Compliance with Ethical Standards

Conflict of interest

The authors declare that they have no conflict of interest.

Funding

This study was funded by NSERC Discovery grant (386360-2010) and *Fonds de Recherche du Québec - Nature et Technologies*.

Ethical approval

All procedures performed in studies involving human participants were in accordance with the ethical standards of the institutional and/or national research committee and with the 1964 Helsinki declaration and its later amendments or comparable ethical standards.

Informed consent

Informed consent was obtained from all individual participants included in the study.

References

1. Achanta, R., Shaji, A., Smith, K., Lucchi, A., Fua, P., Susstrunk, S.: Slic superpixels compared to state-of-the-art superpixel methods. Pattern Analysis and Machine Intelligence, IEEE Transactions on **34**(11), 2274–2282 (2012)
2. Ahmadi, N., Shavelle, D., Nabavi, V., Hajsadeghi, F., Moshrefi, S., Flores, F., Azmoon, S., Mao, S.S., Ebrahimi, R., Budoff, M.: Coronary distensibility index measured by computed tomography is associated with the severity of coronary artery disease. Journal of cardiovascular computed tomography **4**(2), 119–126 (2010)
3. Benovoy, M., Cheriet, F., Maurice, R.L., Dahdah, N.: Automated angiographic assessment of coronary artery vasomotion in kawasaki disease patients. Circulation **131**(Suppl 2), A153–A153 (2015)
4. Benovoy, M., Dionne, A., Cheriet, F., Maurice, R.L., Dahdah, N.: Correlation between automatic angio-based coronary artery stiffness assessment and visual oct pathology scoring. Journal of the American College of Cardiology **67**(13_S), 1672–1672 (2016)
5. Bouix, S., Siddiqi, K., Tannenbaum, A.: Flux driven automatic centerline extraction. Medical Image Analysis **9**(3), 209–221 (2005)
6. Cheung, Y., Brogan, P., Pilla, C., Dillon, M., Redington, A.: Arterial distensibility in children and teenagers: normal evolution and the effect of childhood vasculitis. Archives of disease in childhood **87**(4), 348–351 (2002)
7. Compas, C., Syeda-Mahmood, T., McNeillie, P., Beymer, D.: Automatic detection of coronary stenosis in x-ray angiography through spatio-temporal tracking. In: Biomedical Imaging (ISBI), 2014 IEEE 11th International Symposium on, pp. 1299–1302 (2014)
8. Frangi, A., Niessen, W., Vincken, K., Viergever, M.: Multiscale vessel enhancement filtering. Medical Image Computing and Computer-Assisted InterventationMICCAI98 p. 130 (1998)

9. Girasis, C., Schuurbiers, J., Muramatsu, T., Aben, J.P., Onuma, Y., Soekhradj, S., Morel, M., van Geuns, R.J., Wentzel, J.J., Serruys, P.W.: Advanced three-dimensional quantitative coronary angiographic assessment of bifurcation lesions: methodology and phantom validation. EuroIntervention **8**(12), 1451–1460 (2013)
10. Grady, L., Sun, Y., Williams, J.: Three interactive graph-based segmentation methods applied to cardiovascular imaging. Handbook of Mathematical Models in Computer Vision pp. 453–469 (2006)
11. Gronenschild, E., Janssen, J., Tijdens, F.: Caas ii: A second generation system for off-line and on-line quantitative coronary angiography. Catheterization and cardiovascular diagnosis **33**(1), 61–75 (1994)
12. Kelle, S., Hays, A.G., Hirsch, G.A., Gerstenblith, G., Miller, J.M., Steinberg, A.M., Schr, M., Texter, J.H., Wellnhofer, E., Weiss, R.G., Stuber, M.: Coronary artery distensibility assessed by 3.0 tesla coronary magnetic resonance imaging in subjects with and without coronary artery disease. The American Journal of Cardiology **108**(4), 491 – 497 (2011)
13. Kroon, D.J., Slump, C., Maal, T.: Optimized anisotropic rotational invariant diffusion scheme on cone-beam ct. In: T. Jiang, N. Navab, J. Pluim, M. Viergever (eds.) Medical Image Computing and Computer-Assisted Intervention MICCAI 2010, *Lecture Notes in Computer Science*, vol. 6363, pp. 221–228. Springer Berlin / Heidelberg (2010)
14. Lesage, D., Angelini, E., Bloch, I., Funka-Lea, G.: A review of 3d vessel lumen segmentation techniques: Models, features and extraction schemes. Medical Image Analysis **13**(6), 819 – 845 (2009). Includes Special Section on Computational Biomechanics for Medicine
15. Maurice, R.L., Vaujois, L., Dahdah, N., Chibab, N., Maurice, A., Nuyt, A.M., Lévy, É., Bigras, J.L.: Carotid wall elastography to assess midterm vascular dysfunction secondary to intrauterine growth restriction: Feasibility and comparison with standardized intima-media thickness. Ultrasound in medicine & biology **40**(5), 864–870 (2014)
16. Medis: Qangio xa. URL http://www.medis.nl/Products/QAngioXA
17. M'hiri, F., Duong, L., Desrosiers, C., Cheriet, M.: Vessel Walker: Coronary arteries segmentation using random walks and hessian-based vesselness filter. In: ISBI, pp. 918–921 (2013)
18. M'hiri, F., Duong, L., Desrosiers, C., Leye, M., Miró, J., Cheriet, M.: A graph-based approach for spatio-temporal segmentation of coronary arteries in x-ray angiographic sequences. Computers in Biology and Medicine **79**, 45–58 (2016)
19. Mirzaalian, H., Hamarneh, G.: Vessel scale-selection using mrf optimization. In: Computer Vision and Pattern Recognition (CVPR), 2010 IEEE Conference on, pp. 3273–3279. IEEE (2010)
20. Otsu, N.: A threshold selection method from gray-level histograms. IEEE Transactions on Systems, Man and Cybernetics **9**(1), 62–66 (1979)
21. PIEMedical: Caas. URL http://www.piemedicalimaging.com/partner/caas/
22. Segars, W.P., Tsui, B.M.: Mcat to xcat: The evolution of 4-d computerized phantoms for imaging research. Proceedings of the IEEE **97**(12), 1954–1968 (2009)
23. Shahzad, R., Kirişli, H., Metz, C., Tang, H., Schaap, M., van Vliet, L., Niessen, W., van Walsum, T.: Automatic segmentation, detection and quantification of coronary artery stenoses on cta. The international journal of cardiovascular imaging **29**(8), 1847–1859 (2013)
24. Shechter, G., Ozturk, C., Resar, J.R., McVeigh, E.R.: Respiratory motion of the heart from free breathing coronary angiograms. Medical Imaging, IEEE Transactions on **23**(8), 1046–1056 (2004)
25. Tomasello, S.D., Galassi, A.R., Costanzo, L.: Advances in the Diagnosis of Coronary Atherosclerosis, chap. Quantitative Coronary Angiography in the Interventional Cardiology, pp. 255–272. INTECH Open Access Publisher (2011)
26. Vaujois, L., Dallaire, F., Maurice, R.L., Fournier, A., Houde, C., Thérien, J., Cartwright, D., Dahdah, N.: The biophysical properties of the aorta are altered following kawasaki disease. Journal of the American Society of Echocardiography **26**(12), 1388–1396 (2013)
27. Weickert, J.: Anisotropic diffusion in image processing, vol. 256. Citeseer (1998)
28. Zhao, M., Lin, H.Y., Yang, C.H., Hsu, C.Y., Pan, J.S., Lin, M.J.: Automatic threshold level set model applied on mri image segmentation of brain tissue. Appl. Math **9**(4), 1971–1980 (2015)
29. Zhu, N., Chung, A.C.: Random walks with adaptive cylinder flux based connectivity for vessel segmentation. In: Medical Image Computing and Computer-Assisted Intervention–MICCAI 2013, pp. 550–558. Springer (2013)